# On the gravity wave forcing during the austral stratospheric final warming as simulated by LMDz

Alvaro de la Cámara[1]* and François Lott

Laboratoire de Météorologie Dynamique, École Normale Supérieure, Paris, France.

[1] Centre de Mathématiques et de Leurs Applications, ENS de Cachan, France.

Valérian Jewtoukoff, Riwal Plougonven and Albert Hertzog

Laboratoire de Météorologie Dynamique, École Polytechnique, Palaiseau, France.

In preparation for submission to Journal of the Atmospheric Sciences.
Version of December 14, 2015

**Abstract**

The austral stratospheric final warming date is often predicted with substantial delay in several climate models. This systematic error is generally attributed to insufficient parametrized gravity waves (GW) drag in the stratosphere around 60°S. This bias is not present in the LMDz general circulation model, a property that we use to analyse the contribution of the different types of waves in the model. For this purpose, the resolved and unresolved wave forcings of the middle atmosphere during the austral spring are examined in LMDz and reanalysis data, and a good agreement is found between the two datasets. The role of parameterized orographic and nonorographic GWs in LMDz is further examined, and it is found that orographic and nonorographic GWs contribute evenly to the GW forcing in the stratosphere, unlike other climate models where orographic GWs are the main contributor. This result is shown to be in good agreement with GW-resolving operational analysis products. It is demonstrated that

*Currently at NCAR, Boulder, Colorado, U.S.A.

the significant contribution of the nonorographic GWs is related to the fact that the source-related nonorographic GW parameterizations used in LMDz produce very intermittent momentum fluxes, in qualitative agreement with recent observations. It yields sporadic high-amplitude events during which the GWs break in the stratosphere and force the circulation at lower altitudes than more homogeneously distributed nonorographic GW parameterization do.

# 1 Introduction

The final warming (FW) of the polar stratosphere marks the transition from the winter to summer circulation conditions, and occurs every spring. It is forced radiatively, but wave-mean flow interactions play an important role and control its inter-annual variability. In the Southern Hemisphere (SH) a number of climate models predicts that it occurs 1–2 weeks later than in observations [Butchart et al., 2011; Eyring et al., 2010; Wilcox and Charlton-Perez, 2013], this systematic error being sometimes accompanied by a cold temperature bias in winter and spring. These biases have important implications on the stratospheric dynamics and chemistry, like a systematic late seasonal ozone recovery over Antarctica that affects simulated long-term ozone trends and Antarctic climate evolution [Barnes et al., 2014; Perlwitz et al., 2008].

The general consensus to explain **these late FW biases** is that climate models **underetimate** the gravity wave (GW) forcing in the southern stratosphere, specially around 60°S [McLandress et al., 2012], but **the** orographic or nonorographic origin **of the missing GWs** is still controversial. In **present day climate** models, this is unavoidably related to how GW parameterizations are constructed. On the one hand, parameterized orographic gravity waves (OGWs) usually break in the troposphere and stratosphere [e.g., Palmer et al., 1986; ?]. This is in contrast to nonorographic gravity waves (NGWs), which are usually treated in the parameterizations as small-amplitude waves, breaking at higher altitudes in the mesosphere to drive the upper branch of the Brewer-Dobson circulation and not interacting directly with the stratospheric flow [e.g. Alexander et al., 2010]. In the atmosphere, OGWs are present around 60°S although the underlying surface is an ocean: there are contributions due to small islands of the Southern Ocean [Alexander et al., 2009; Alexander and Grimsdell, 2013] and due to lateral propagation from the Andes and the Antarctic Peninsula [Sato et al., 2012, 2009]. However, small islands are absent or dwarved because of poor resolution in climate models, and horizontal propagation is absent from nearly all parameterizations by construction, leading to a gap in parameterized OGW drag around 60°S. Although this gap is unphysical, this does not imply that OGWs are solely responsible for the missing GW drag (GWD), as suggested by McLandress et al. [2012]. Another possibility may be that NGWs are often parameterized as small perturbations, implying that they can propagate to high altitudes before dissipating. This is also unrealistic according to the recent observational studies that emphasize the intermittent character of the GW momentum fluxes entering the SH stratosphere [Alexander, 2015; Hertzog et al., 2012, 2008; Plougonven et al., 2013; Wright et al., 2013], and this intermittency is absent from nearly all GW parametrizations. If taken into account, this intermittency could make the NGWs contribute to the missing GWD more substantially than usually believed.

From the observational side, some studies using satellite-derived products have demonstrated that GWs generated by flow over the small southern islands can carry a significant amount of momentum flux [e.g., Alexander et al., 2009; Alexander and Grimsdell, 2013], but the expected contribution to the global-scale forcing is presumably modest. Other works have pointed out that the stratospheric GWs observed over the ocean surrounding Antarctica likely have nonorographic sources. Hendricks et al. [2014] studied the source of the stratospheric GW belt (at around 60°S) in austral winter. They found a strong correlation between GW activity and mid-tropospheric maximum Eady growth rate, suggesting the nonorographic origin of the GWs. In a recent study, Jewtoukoff et al. [2015] showed quantitative evidences from in-situ balloon observations and high-resolution ECMWF operational analyses that the momentum flux around 60°S in the lower stratosphere in spring is dominated by GWs from nonorographic sources [see also Hertzog et al., 2008; Plougonven et al., 2013]. Using observations of the first mesosphere-stratosphere-troposphere radar in Antarctica, Shibuya et al. [2015] also stress the important contribution of nonorographic GWs to the total momentum flux in the austral lower stratosphere.

The goal of the present study is to contribute to the debate by analyzing the wave forcing during the final warming of the southern stratosphere in climate simulations with the Laboratoire de Météorologie Dynamique general circulation model with zoom (LMDz), and in reanalysis products. LMDz includes state-of-the-art stochastic parameterizations of nonorographic GWs tied to their tropospheric sources [de la Cámara and Lott, 2015; Lott and Guez, 2013], which generate lognormally distributed momentum fluxes in agreement with observations [de la Cámara et al., 2014; Jewtoukoff et al., 2015], as well as orographic gravity waves [Lott, 1999; **?**]. As a result, we will show that the contribution to the total GW drag in the stratosphere of nonorographic GWs is larger than that reported in previous studies with different parameterizations, and no significant bias on the FW date is found in our model. We will also show that the ratio of OGWD to NGWD parameterized in LMDz is qualitatively realistic as compared to the GW-resolving European Centre for Medium-Range Forecast (ECMWF) operational analysis.

The paper is organized as follows. Section 2 presents the LMDz model, the method used to infer the GWD from reanalysis fields, and the calculation of GWD from the ECMWF operational analysis. In section 3 we analyse the wave forcing during the final warming of the SH, with emphasis on the unresolved waves, and investigate the role of parameterized GW intermittency. The main conclusions are given in section 4.

# 2 Model and methodology

## 2.1 LMDz general circulation model

The LMDz version we use has a 3.75°×1.875° longitude-latitude grid, and 71 levels in the vertical with the top at 1 Pa, and a vertical resolution of around 1 km in the lower stratosphere. We show results from a control run of 20 years, forced with climatological fields of sea surface temperature, sea ice, soil temperature and composition over land.

LMDz uses three distinct GWD parameterizations, representing GWs generated by subgrid-scale orography [Lott, 1999], by convection [Lott and Guez, 2013], and by fronts [de la Cámara and Lott, 2015]. The last two are stochastic and supposed to cover all the GWs of nonorographic origins. de la Cámara et al. [2014] and de la Cámara and Lott [2015]showed that the combination of a stochastic approach and the relation with the sources produce lognormally distributed momentum fluxes, i.e. including large, rare events that account for much of the mean value and that potentially break at lower altitudes in the stratosphere.

## 2.2 Inferring gravity wave drag from reanalysis

The zonal mean momentum balance in the Transformed Eulerian Mean (TEM) formalism is given by:

$$\frac{\partial \bar{u}}{\partial t} = \left\{ \frac{\vec{\nabla} \cdot \vec{F}}{\rho_0 a \cos\phi} + \bar{X} \right\} + \left\{ \bar{v}^* \hat{f} - \bar{w}^* \frac{\partial \bar{u}}{\partial z} \right\} + residual, \tag{1}$$

where $a$ is the Earth radius, $\phi$ is latitude, $z = -H \log(p/p_r)$ is the log-pressure altitude, $\rho_0 = \rho_r e^{-z/H}$ is the background density, $\hat{f} = f - \frac{1}{a\cos\phi}\frac{\partial(\bar{u}\cos\phi)}{\partial\phi}$ with $f$ the Coriolis parameter, $\vec{F}$ is the Eliassen-Palm (EP) flux, and $(\bar{v}^*, \bar{w}^*)$ is the TEM residual circulation [Andrews et al., 1987]. In Eq. 1 the zonal mean wind tendency is determined by the total wave forcing (the first set of braces) and the advection term (the second set of braces). The total wave forcing consists of the divergence of the resolved EP flux $\vec{F}$ and the drag imposed by parameterized

GWs ($\bar{X}$).

In the present study we will use the TEM formalism to infer the GWD from ERA-Interim (ERAI) daily averaged data [Dee and et al, 2011]. We will consider that Eq. 1 will generally not be balanced in reanalysis products (the residual will be non-negligible) due to the assimilation process and the resulting analysis increments. For the target region and time of the year it is reasonable to assume that the analysis increments are mainly caused by insufficient parameterized GWD [McLandress et al., 2012]. Similarly to Alexander and Rosenlof [2003] and Ern et al. [2014], we calculate the total GWD in ERAI ($\bar{X}_{res}$):

$$\bar{X}_{res} = \frac{\partial \bar{u}}{\partial t} - \frac{\vec{\nabla} \cdot \vec{F}}{\rho_0 a \cos\phi} - \left\{ \bar{v}^* \hat{f} - \bar{w}^* \frac{\partial \bar{u}}{\partial z} \right\}, \quad (2)$$

which is equivalent to the sum of the parameterized GWD and the residual of Eq. 1 ($\bar{X}_{res} = \bar{X} + residual$):

## 2.3 Gravity wave drag from ECMWF operational analysis data

The ECMWF model used to prepare operational analyses 4 times a day and to make weather predictions has a spectral truncation of T1279 and 91 vertical levels, corresponding to a grid spacing of around 500m in the free troposphere and stratosphere. At these resolutions, it is expected that a significant fraction of the GWs is resolved, and we know from Ern et al. [2008], Shutts and Vosper [2011] and Preusse et al. [2014] that the GWs in the ECMWF operational analysis fairly compare to those observed by satellites, a result confirmed with in-situ super pressure balloons [Jewtoukoff et al., 2015]. Relevant for our work, Jewtoukoff et al. [2015] showed that the spatial distribution of the GWs in the analysis is realistic as well as the wave statistics.

In the present study, we will use the ECMWF operational analysis data to diagnose the ratio of OGW drag to NGW drag and consider for this the data available four times a day (0h, 6h, 12h, and 18h UTC) over a 5 year period (2006–2010). Following Jewtoukoff et al. [2015], the GW velocity perturbations are obtained by spectral truncation of the wind and temperature field removing the 15 first zonal modes. In the spectral space the density and local correlations between the zonal and vertical components of the wind, and the meridional wind and temperature, are calculated to yield the vertical component of the E-P flux:

$$\mathrm{F}^{(\mathrm{z})} = \rho_0 a \cos\phi \left[ \left( f - \frac{1}{a\cos\phi} \frac{\partial \bar{u}\cos\phi}{\partial\phi} \right) \frac{\overline{v'\theta'}}{\partial\bar{\theta}/\partial z} - \overline{w'u'} \right]. \tag{3}$$

The vertical divergence of the flux gives the resolved GW drag. It is important to remark that ERA-Interim data is used in the present study to analyze the unresolved wave drag in a consistent climatological dataset, while the ECMWF operational analysis data is used to explore the balance between orographic and nonorographic GW drag in a GW-resolving dataset.

# 3 Results

## 3.1 The austral stratospheric final warming in LMDz

Figures 1a-b illustrate the austral stratospheric final warming in ERAI through a climatological average (1979-2012) of the altitude-time evolution of the zonal mean zonal wind at 70S-50S and temperature over the polar cap during the southern winter and spring. The latitude range for the wind corresponds to the approximate location of the jet maximum throughout the season. During the winter months the wind is eastward, with a maximum of ∼70 m·s$^{-1}$ in July around 1 hPa and below. Starting in late September and from the highest altitudes, the winds decelerate and change to westward direction, signaling the transition from winter to summer circulation conditions. The black contour in Fig. 1a represents the zero-wind line, and the gray contour the 10 m/s wind line, and illustrate very clearly that the transition from eastward to westward winds happens at mesospheric levels first (in October above 1 hPa) and at stratospheric levels later in the season (in early December at 10 hPa). The transition in temperature appears lower down and about a month earlier, with a warming of several tens of degree in agreement with early studies of the FW [e.g.

Mechoso et al., 1985]. Figures 1c,d show similar plots but for LMDz. The maximum of the winter jet (80 m·s$^{-1}$) is stronger than in ERAI, and the very low temperatures in the winter lower stratosphere slightly expand to lower levels. Apart from these differences, the evolution of the zonal wind and temperature simulated by LMDz compares well with that reproduced in ERAI. Following Black and McDaniel [2007], we use 5-day running averages of daily data to calculate the final warming date as the final time that the zonal-mean zonal wind at 60°S and 50 hPa drops below 10-m·s$^{-1}$ until the following autumn. As shown in Fig. 1, the averaged final warming date is the 342 day-of-year in ERAI, and the 348 day-of-year in LMDz (day 343 in a 360-day year), which are fairly close to each other.

Figure 2 gives a complementary view of the zonal wind evolution over the spring, displaying the monthly zonal-mean zonal wind for September, October and November in ERAI and LMDz. There is reasonable agreement between the two datasets, in particular the position of the zero-wind line. These results illustrate that LMDz does a good job simulating the final warming of the SH. In the next sections we analyze the resolved and unresolved wave forcing during the FW, focusing on the role of nonorographic GW parameterizations.

## 3.2 Resolved and unresolved wave forcing

Figure 3 shows latitude-height cross-sections of monthly mean resolved wave drag (i.e. divergence of the EP flux, DF) in ERAI and LMDz, for October and November from the mid-stratosphere to the lower mesosphere. In October, the magnitude and the extent of the negative wave forcing in ERAI resembles that in LMDz (Figs. 3a,c). The main difference appears over the pole higher than 0.3 hPa, where the positive values are larger in ERAI. This positive EP flux divergence arises in a region of very weak positive and negative winds (Fig. 2b,e), where the waves tend to be refracted away resulting in positive divergence of the EP flux. The difference in magnitude could be partly due to a weaker vertical shear in ERAI than in LMDz, which favors refraction. In November as well, the forcing is similar in both datasets, with slightly stronger negative forcing in LMDz than in ERAI in the stratosphere (below ∼1 hPa).

Figures 4a-d show the corresponding latitude-height cross-sections of monthly mean $\bar{X}_{res}$ in ERAI and total GWD in LMDz. Interestingly, the momentum-balance estimate for the GWD in ERAI shows clear similarities with the parameterized GWD in LMDz in both magnitude and distribution. There is strong negative forcing in mid- to high latitudes in October that weakens in November, but the -1 m $s^{-1}$ $d^{-1}$ isoline expands to lower altitudes in the stratosphere in ERAI than in LMDz. Although a bit weaker, the GW forcing has a similar pattern and order of magnitude in October and November as that of the resolved waves (Fig. 3), highlighting the importance of GW drag parameterizations to achieve a realistic middle atmospheric circulation.

It is interesting that despite the different horizontal resolutions, ERAI having a horizontal spacing of about 80 km (T255 spectral truncation) and LMDz of about 200 km, the resolved and unresolved wave forcing have a similar order of magnitude and latitude distribution in both datasets. The reason is probably that the resolved forcing in the stratosphere in both ERAI and LMDz essentially come from planetary scale Rossby waves, e.g. waves with scales that can be resolved in both models, and consistent with the fact that the synoptic disturbances play a small role in the middle atmosphere dynamics [Andrews et al., 1987].

## 3.3 Orographic and nonorographic gravity wave drag

We next analyse the relative contribution of the nonorographic and orographic GWD parameterizations to the total GW forcing in LMDz. Figure 5 shows the profiles of OGWD and NGWD for October, focusing on stratospheric levels from 100 to 1 hPa. It appears that the main contribution to the total GW forcing at these altitudes in the model comes from nonorographic GWs. The OGWD presents a minimum around 60°S consistent with the absence of topography in that latitude band and the columnar approximation made in parameterizations. This gap of orographic GWD at 60°S is compensated by GWD of nonorographic origin, which peaks around that latitude possibly due to the location of the tropospheric sources [Hendricks et al., 2014] and the presence of the stratospheric jet. This relatively large contribution in LMDz of nonorographic GWs to the stratospheric forcing during the austral spring differs from most climate models. In a study of the SH cold pole and strong jet biases in the Canadian Middle Atmosphere Model, McLandress et al. [2012] showed that the OGWD was much stronger than the NGWD in their model, and found that the mentioned biases were reduced when including an extra forcing at 60°S in the OGWD scheme.

Recent observations indicate that the GW momentum flux in the springtime lower stratosphere over the Southern Ocean is dominated by nonorographic GWs [e.g., Hendricks et al., 2014; Jewtoukoff et al., 2015; Shibuya et al., 2015], pointing to the potential importance of these waves in forcing the stratospheric circulation in the region. However, this cannot be verified observationally since the derivation of the GW drag from global measurements remains a big challenge [Alexander, 2015; Geller et al., 2013]. Thus, to address whether the balance between orographic and nonorographic GWD in LMDz is consistent, we next compare the GW drag in LMDz with the GW drag obtained from the resolved spectrum of GWs in the ECMWF operational model (see Section 2). Figure 6 shows the corresponding plots for ECMWF operational analyses data. We simply apply a geographical mask to discern between orographic and nonorographic GWs: all the GWs placed over the green areas in Fig. 6c will be considered most likely of orographic origin, and those outside the green areas almost surely of nonorographic origin. Using a GW resolving climate model, Sato et al. [2012] showed that OGWs originating from the Andes and Antarctic Peninsula propagate very far leeward of the topographic obstacles. To account for this effect, our 'orographic' region extends downstream of obstacles as in Plougonven et al. [2013]. The OGWD in the analyses (Fig. 6a) does not go to zero around 60°S, unlike in LMDz(Fig. 5a). This is clearly due to the fact that we consider as orographic GWs those detected above small islands and over a vast region leeward of the Andes and Antarctic Peninsula (Fig. 6c). Apart from this difference, the magnitude and vertical extension of OGWD and NGWD agree reasonably well with parameterized data in LMDz. And importantly, the ratio of OGWD to NGWD is similar in both datasets.

### 3.4 The role of gravity wave intermittency

To clarify further the significance of the intermittency, we next make offline tests using October daily fields from LMDz, and test different configuration of the NGWD schemes. Figure 7a presents the NGW drag averaged in time and longitude. It compares well with the online runs in Fig. 5b, witnessing the potential of the offline calculations. First, these offline runs permit to estimate the intermittency of the momentum-flux predicted by our schemes, as Fig. 7b illustrates by showing the probability density functions of NGW absolute momentum flux at different levels in the stratosphere south of 40°S (Fig. 7b). As highlighted in de la Cámara et al. [2014] and de la Cámara and Lott [2015], the NGW sources included in these stochastic parameterizations naturally generate lognormally distributed momentum fluxes in agreement with observations [Alexander, 2015; Hertzog et al., 2012; Jewtoukoff et al., 2015]. We see in Fig. 7b that the larger, less frequent momentum fluxes are filtered out throughout the stratosphere, and therefore are responsible for the NGW drag at stratospheric levels.

To reveal more precisely the significance of intermittency, we next run our NGWs parameterization imposing a constant flux at the launching altitude, and choose for value the averaged of the flux amplitude emitted when the sources are explicit. The value is near 3 mPa, and the corresponding drag due to the westward component of the GW stress is shown in Fig. 8, where the bottom panels show the drag multiplied by a normalized density to highlight the values at stratospheric levels. The westward drag produced when considering a fixed emitted stress of 3 mPa is smaller in the stratosphere and larger in the mesosphere than when considering NGW sources (Figs. 8a, 8b, 8c, and 8d).

The differences at mesospheric levels are important. As commented in the Introduction, NGW parameterization were introduced in climate models to be active at high altitudes, in order to close the mesospheric jets and to contribute to the upper branch of the Brewer-Dobson circulation. Therefore, as our model with source-related NGWs is quite realistic, it is likely that one should reduce the imposed fixed stress to reach comparable results online with fixed stress. This is therefore what is done in Figs. 8c and 8f, which show the westward wave drag for an offline run reducing the emitted fixed stress to 1.25 mPa. We obtain now a reasonable drag above 50 km, but at the cost of reducing significantly the drag in the stratosphere.

To summarize, these results suggest that with schemes imposing fixed NGWs sources it will be difficult to predict the stratospheric GW drag requested to simulate the annual cycle of the westerly jet without altering the mesosphere.

# 4 Summary and conclusions

Insufficient parameterized GW drag around 60°S is likely causing the delay in springtime breakdown of the austral polar vortex in a number of climate models [e.g., Wilcox and Charlton-Perez, 2013]. Yet, there is not a clear consensus on the origin of the 'missing' GW drag (orographic versus nonorographic) [e.g., McLandress et al., 2012]. Recent observational studies stress the significant contribution of nonorographic GWs to the total momentum flux in the lower stratosphere, and highlight their intermittent behaviour [e.g., Alexander, 2015; Hendricks et al., 2014; Hertzog et al., 2012; Jewtoukoff et al., 2015; Shibuya et al., 2015; Wright et al., 2013]. This intermittency decisively determines the altitude at which the waves break, and is generally not modelled in NGW parameterizations.

We have shown that the LMDz climate model does not present a significant delay of the stratospheric vortex breakdown, and consequently can be used to analyze the wave forcing during the austral stratospheric final warming. We have found a good agreement in the zonal drag exerted by resolved and unresolved waves between LMDz and ERAI. In LMDz, the unresolved forcing comprises the parameterized GW drag (i.e orographic, convective and frontal GWs), while in ERAI it has been derived from the momentum balance in the

Transformed Eulerian Mean formalism.

Differently from many climate models, where orographic GWs play a dominant role at stratospheric levels, the parameterized GW drag in LMDz during the austral final warming is not larger for waves of orographic origin than for those of nonorographic origin. Furthermore, while the OGW drag presents a minimum at 60°S, the NGW drag presents a maximum at this latitude possibly related to baroclinic activity and favourable propagation conditions in the jet stream. Therefore, in LMDz nonorographic GWs make a significant contribution to the total wave forcing during the austral final warming. We have demonstrated that this significant contribution of NGWs at stratospheric levels is due to a qualitatively realistic representation of momentum-flux intermittency in the NGW parameterizations used. The stochastic scheme, tied to convective and frontal GW sources [de la Cámara and Lott, 2015; Lott and Guez, 2013], naturally produce sporadic, high-amplitude GWs that tend to break and force the circulation at lower levels in the stratosphere. At the same time, the bulk of waves carrying small momentum flux produce a drag in the mesosphere that keep simulated winds and temperature at those altitudes within reasonable limits.

Using resolved gravity waves from the high-resolution ECMWF operational analysis, we have shown that the balance between orographic and nonorographic GW drag is similar to the drag parameterized in LMDz, which provides a physical justification for a fair representation of momentum-flux intermittency in nonorographic GW parameterizations. We know that the ECMWF operational analysis underestimates by a factor of 5 the resolved GW momentum fluxes entering in the stratosphere when compared to direct balloon measurements Jewtoukoff et al. [2015]. Although we have shown that the introduction of intermittency permits us to increase substantially the GW fluxes entering the model stratosphere without degrading the mesosphere, these quite large measured values tell that much more still needs to be understood concerning the drag exerted in the models' stratosphere at lower levels. Also, we must not forget that the necessary simplifications made in parameterizations, such as instant vertical propagation or total conversion of vertical momentum flux into a drag, could be missing some fundamental dynamics that might explain the large quantitative deviations between the observed absolute momentum fluxes in the lower stratosphere [Alexander, 2015; Jewtoukoff et al., 2015], and the parameterized values (see Fig. 7b). In this regard, the direct comparison of observed and modelled (parameterized) momentum fluxes might not be well-posed [Geller et al., 2013].

Finally, our results do not rule out the potential role of misrepresented orographic GWs due to the absence of lateral propagation in the parameterizations [see Kalisch et al., 2014]. We rather argue that it is not the only cause of the GW drag deficit, and that the missing drag can be to a great extent due to nonorographic GWs. Also, we argue that improving the NGWs parameterizations by relating quantitatively the GW amplitudes to their sources can help to simulate better the Antarctic stratospheric final warming.

**Acknowledgements**:

The authors would to thank the French ANR project Stradyvarius (Stratospheric Dynamics and Variability), and the Franco-Argentinian LEFE and ECOS projects DIAC (Dynamical Influence of the Andes on Climate) and DIAGAC (Dynamical Influence of the Andes on the Global and Argentinian Climate). AdlC has been partially supported by the Advanced Study Program at NCAR.

# References

Alexander, M. J. (2015). Global and seasonal variations in three-dimensional gravity wave momentum flux from satellite limb-sounding temperatures. Geophysical Research Letters, 42(16):6860–6867. 2015GL065234.

Alexander, M. J., Eckermann, S. D., Broutman, D., and Ma, J. (2009). Momentum flux estimates for south giorgia island mountain waves in the stratosphere observed via satellite. Geophysical Research Letters, 36:L12816.

Alexander, M. J., Geller, M., McLandress, C., Polavarapu, S., P. Preusse, P., Sassi, F., Sato, K., Eckermann, S., Ern, M., Hertzog, A., Kawatani, Y., Pulido, M., Shaw, T. A., Sigmond, M., Vincent, R., and Watanabe,

S. (2010). Recent developments in gravity-wave effects in climate models and the global distribution of gravity-wave momentum flux from observations and models. Quarterly Journal of the Royal Meteorological Society, 136:1103–1124.

Alexander, M. J. and Grimsdell, A. W. (2013). Seasonal cycle of orographic gravity wave ocurrence above small islands in the southern hemisphere: Implications for effects on the general circulation. Journal of Geophysical Research Atmospheres, 118:11589–11599.

Alexander, M. J. and Rosenlof, K. H. (2003). Gravity-wave forcing in the stratosphere: Observational constraints from the upper atmosphere research satellite and implications for parameterization in global models. Journal of Geophysical Research, 108:4597.

Andrews, D. G., Holton, J. R., and Leovy, C. B. (1987). Middle atmosphere dynamics. Academic Press. 489 pp.

Barnes, E. A., Barnes, N. W., and Polvani, L. M. (2014). Delayed southern hemisphere climate change induced by stratospheric ozone recovery, as projected by the cmip5 models. Journal of Climate, 27:852–867.

Black, R. W. and McDaniel, B. A. (2007). Interannual variability in the southern hemisphere circulation organized by stratospheric final warming events. Journal of the Atmospheric Sciences, 64:2968–2974.

Butchart, N., Charlton-Perez, A. J., Cionni, I., Hardiman, S. C., Haynes, P. H., Krüger, K., Kushner, P. J., Newman, P. A., Osprey, S. M., Perlwitz, J., Sigmond, M., Wang, L., Akiyoshi, H., J., A., Bekki, S., Baumgaertner, A., Braesicke, P., Brühl, C., Chipperfield, M., Dameris, M., Dhomse, S., Eyring, V., Garcia, R., Garny, H., Jöckel, P., Lamarque, J.-F., Marchand, M., Michou, M., Morgenstern, O., Nakamura, T., Pawson, S., Plummer, D., Pyle, J., E., R., Scinocca, J., Shepherd, T. G., Shibata, K., Smale, D., Teyssedre, H., Tian, W., Waugh, D., and Yamashita, Y. (2011). Multimodel climate and variability of the stratosphere. Journal of Geophysical Research, 116:D05102.

de la Cámara, A. and Lott, F. (2015). A stochastic parameterization of the gravity waves emitted by fronts and jets. Geophysical Research Letters, 42:2071–2078.

de la Cámara, A., Lott, F., and Hertzog, A. (2014). Intermittency in a stochastic parameterization of nonorographic gravity waves. Journal of Geophysical Research Atmospheres, 119:11905–11919.

Dee, D. P. and et al (2011). The era-interim reanalysis: Configuration and performance of the data assimilation system. Quarterly Journal of the Royal Meteorological Society, 137:553–597.

Ern, M., Ploeger, F., Preusse, P., Gille, J. C., Gray, L. J., Kalisch, S., Mlynczak, M. G., Russell III, J. M., and Riese, M. (2014). Interaction of gravity waves with the qbo: A satellite perspective. Journal of Geophysical Research Atmospheres, 119:2329–2355.

Ern, M., Preusse, P., Krebsbach, M., Mlynczak, M. G., and Russell III, J. M. (2008). Equatorial wave analysis from saber and ecmwf temperatures. Atmos. Chem. Phys., 8:845–869.

Eyring, V., Shepherd, T. G., and Waugh, D. W., editors (2010). Evaluation of Chemistry-Climate Models. Number Rep. 5, WCRP-132. Geneva, Switzerland.

Geller, M. A., Alexander, M. J., Love, P. T., Bacmeister, J., Ern, M., HERTZOG, A., Manzini, E., Preusse, P., Sato, K., Scaige, A. A., and Zhou, T. (2013). A comparison between gravity wave momentum fluxes in observations and climate models. Journal of Climate, 26:6383–6405.

Hendricks, E. A., Doyle, J. D., Eckermann, S. D., Jiang, Q., and Reinecke, P. A. (2014). What is the source of the stratospheric gravity wave belt in austral winter? Journal of the Atmospheric Sciences, 71:1583–1592.

Hertzog, A., Alexander, M. J., and Plougonven, R. (2012). On the intermittency of gravity wave momentum flux in the stratosphere. Journal of the Atmospheric Sciences, 69:3433–3448.

Hertzog, A., Boccara, G., Vincent, R. A., Vial, F., and Cocquerez, P. (2008). Estimation of gravity wave momentum flux and phase speeds from quasi-lagrangian stratospheric balloon flights. part ii: Results from the vorcore campaign in antarctica. Journal of the Atmospheric Sciences, 65:3056–3070.

Jewtoukoff, V., Hertzog, A., Plougonven, R., de la Cámara, A., and Lott, F. (2015). Gravity waves in the southern hemisphere derived from balloon observations and the ecmwf analyses. Journal of the Atmospheric Sciences.

Kalisch, S., Preusse, P., Ern, M., Eckermann, S. D., and Riese, M. (2014). Differences in gravity wave drag between realistic oblique and assumed vertical propagation. Journal of Geophysical Research Atmospheres, 119.

Lott, F. (1999). Alleviation of stationary biases in a gcm through a mountain drag parameterization scheme and a simple representation of mountain lift forces. Monthly Weather Review, 127:788–801.

Lott, F. and Guez, L. (2013). A stochastic parameterization of the gravity waves due to convection and its impact on the equatorial stratosphere. Journal of Geophysical Research Atmospheres, 118:8897–8909.

McLandress, C., Shepherd, T. G., Polavarapu, S., and Beagley, S. R. (2012). Is missing orographic gravity wave drag near 60s the cuase of the stratospheric zonal wind biases in chemistry-climate models? Journal of the Atmospheric Sciences, 69:802–818.

Mechoso, C. R., Hartmann, D. L., and Farrara, J. D. (1985). Climatology and interanual variability of wave, mean-flow interaction in the southern hemisphere. Journal of the Atmospheric Sciences, 42:2189–2206.

Palmer, T. N., Shutts, G. J., and Swinbank, R. (1986). Alleviation of a systematic westerly bias in general circulation and numerical weather prediction models through an orographic gravity wave drag parametrization. Quarterly Journal of the Royal Meteorological Society, 112(474):1001–1039.

Perlwitz, J., Pawson, S., Fogt, R. L., Nielsen, J. E., and Neff, W. D. (2008). Impact of stratospheric ozone hole recovery on antarctic climate. Geophysical Research Letters, 35:L08714.

Plougonven, R., Hertzog, A., and Guez, L. (2013). Gravity waves over antarctica and the southern ocean: Consistent momentum fluxes in mesoscale simulations and stratospheric balloon observations. Quarterly Journal of the Royal Meteorological Society, 139:101–118.

Preusse, P., Ern, M., Bechtold, P., Eckermann, S. D., Kalisch, S., Trinh, Q. T., and Riese, M. (2014). Characteristics of gravity waves resolved by ecmwf. Atmospheric Chemistry and Physics, 14:10483–10508.

Sato, K., Tateno, S., Watanabe, S., and Kawatani, Y. (2012). Gravity wave characteristics in the southern hemisphere revealed by a high-resolution middle-atmosphere general circulation model. J. Atmos. Sci., 69:1378–1396.

Sato, K., Watanabe, S., Kawatani, Y., Tomikawa, Y., Miyazaki, K., and Takahashi, M. (2009). On the origins of mesospheric gravity waves. Geophysical Research Letters, 36:L19801.

Shibuya, R., Sato, K., Tomikawa, Y., Tsutsumi, M., and Sato, T. (2015). A study of multiple tropopause structures caused by inertiagravity waves in the antarctic. J. Atmos. Sci., 72:2109–2130.

Shutts, G. J. and Vosper, S. B. (2011). Stratospheric gravity waves revealed in nwp model forecasts. Quarterly Journal of the Royal Meteorological Society, 137:303–317.

Wilcox, L. J. and Charlton-Perez, A. J. (2013). Final warming of the southern hemisphere polar vortex in high- and low-top cmip5 models. Journal of Geophysical Research Atmospheres, 118:2535–2546.

Wright, C. J., Osprey, S. M., and Gille, J. C. (2013). Global observations of gravity wave intermittency and its impact on the observed momentum flux morphology. Journal of Geophysical Research Atmospheres.

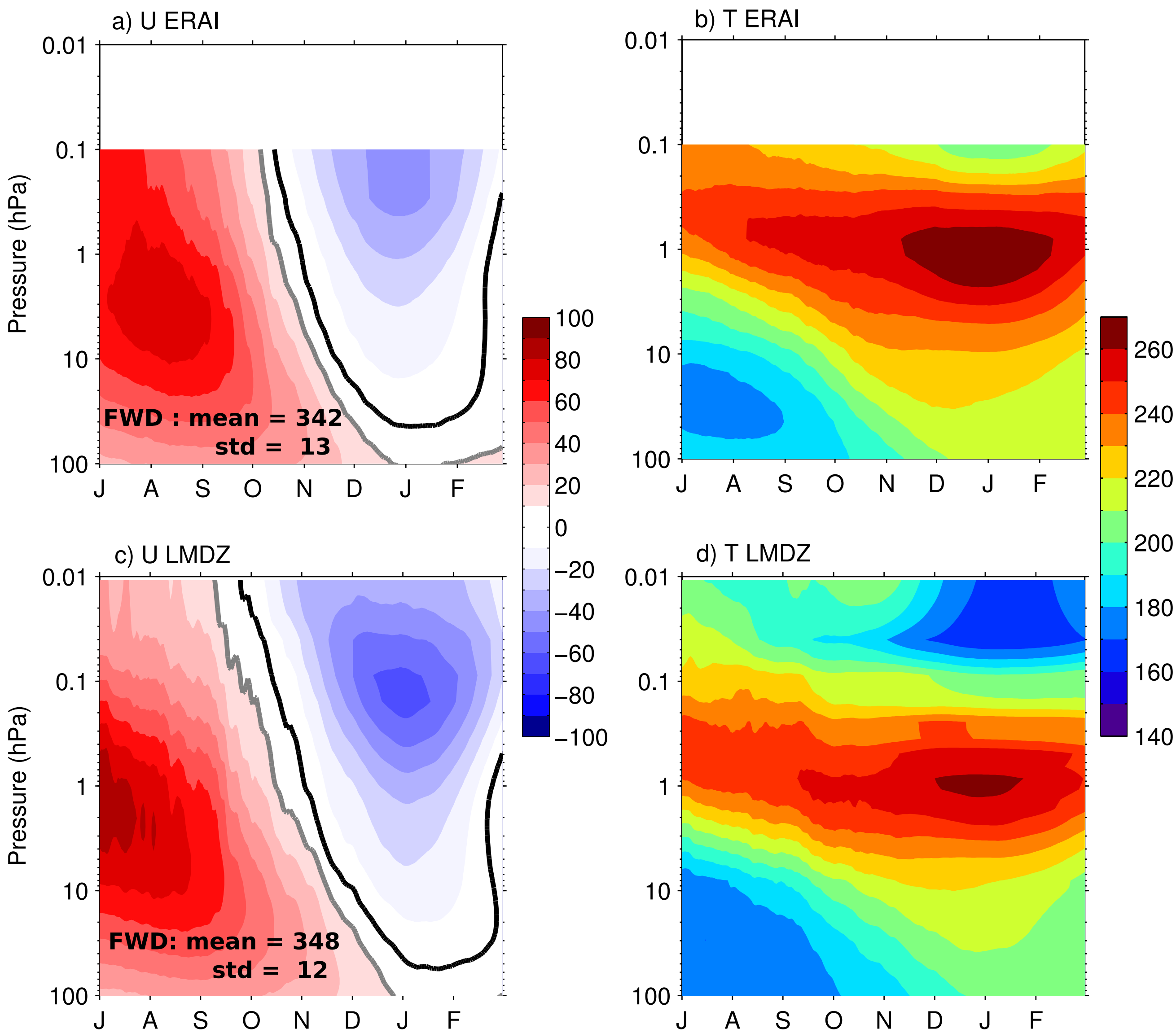


Figure 1: Time-height evolution of (a) zonal mean zonal wind averaged over 70°S-50°S and (b) temperature averaged over 85°S-60°S during the southern winter and spring for ERAI. (c, d) Same as (a, b) but for LMDz. The averaged date of the final warming, and the standard deviation (in Julian days) are also indicated for each dataset.

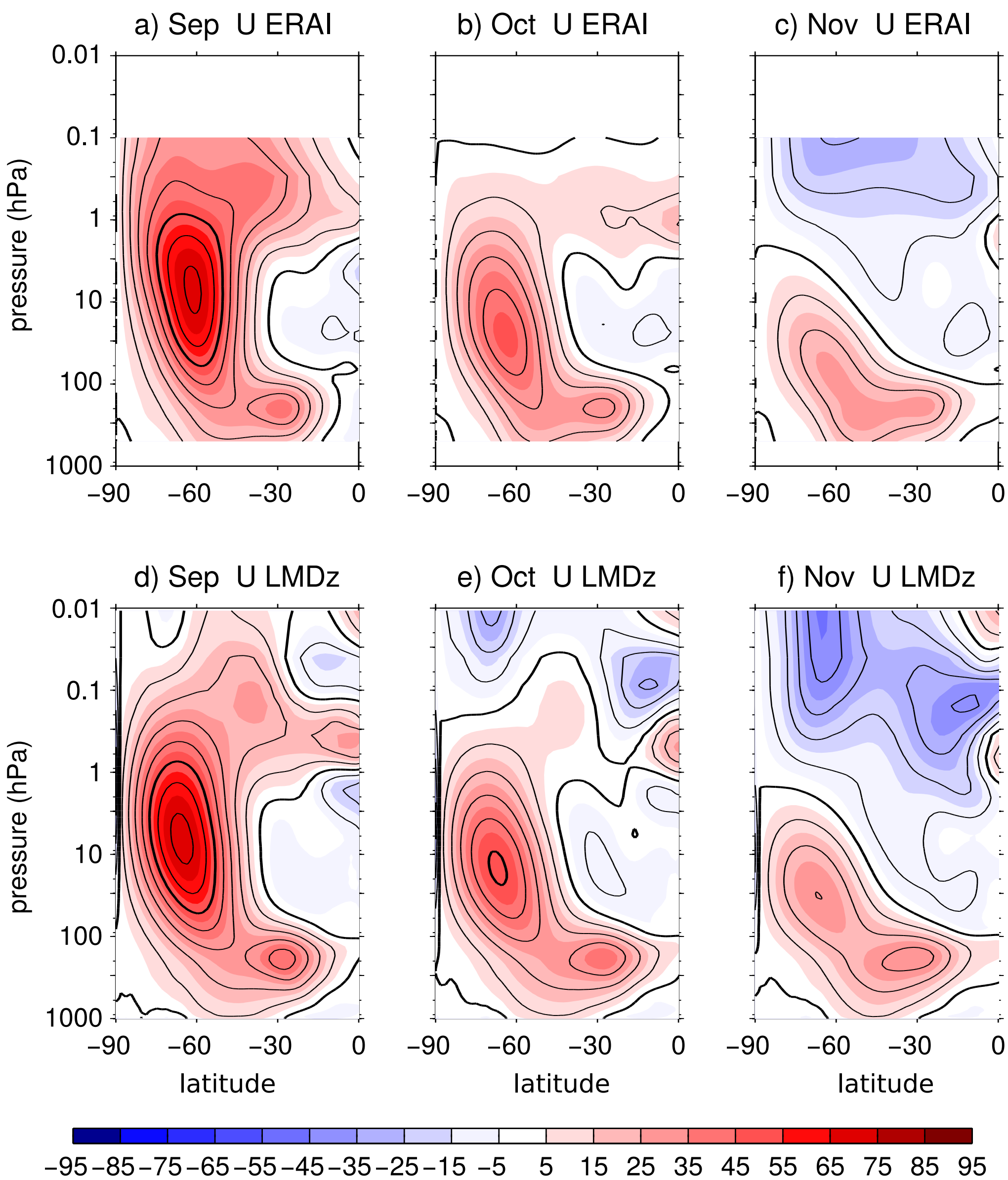


Figure 2: Time-height evolution of (a) zonal mean zonal wind averaged over 70°S-50°S and (b) temperature averaged over 85°S-60°S during the southern winter and spring for ERAI. (c, d) Same as (a, b) but for LMDz. The averaged date of the final warming, and the standard deviation (in Julian days) are also indicated for each dataset.

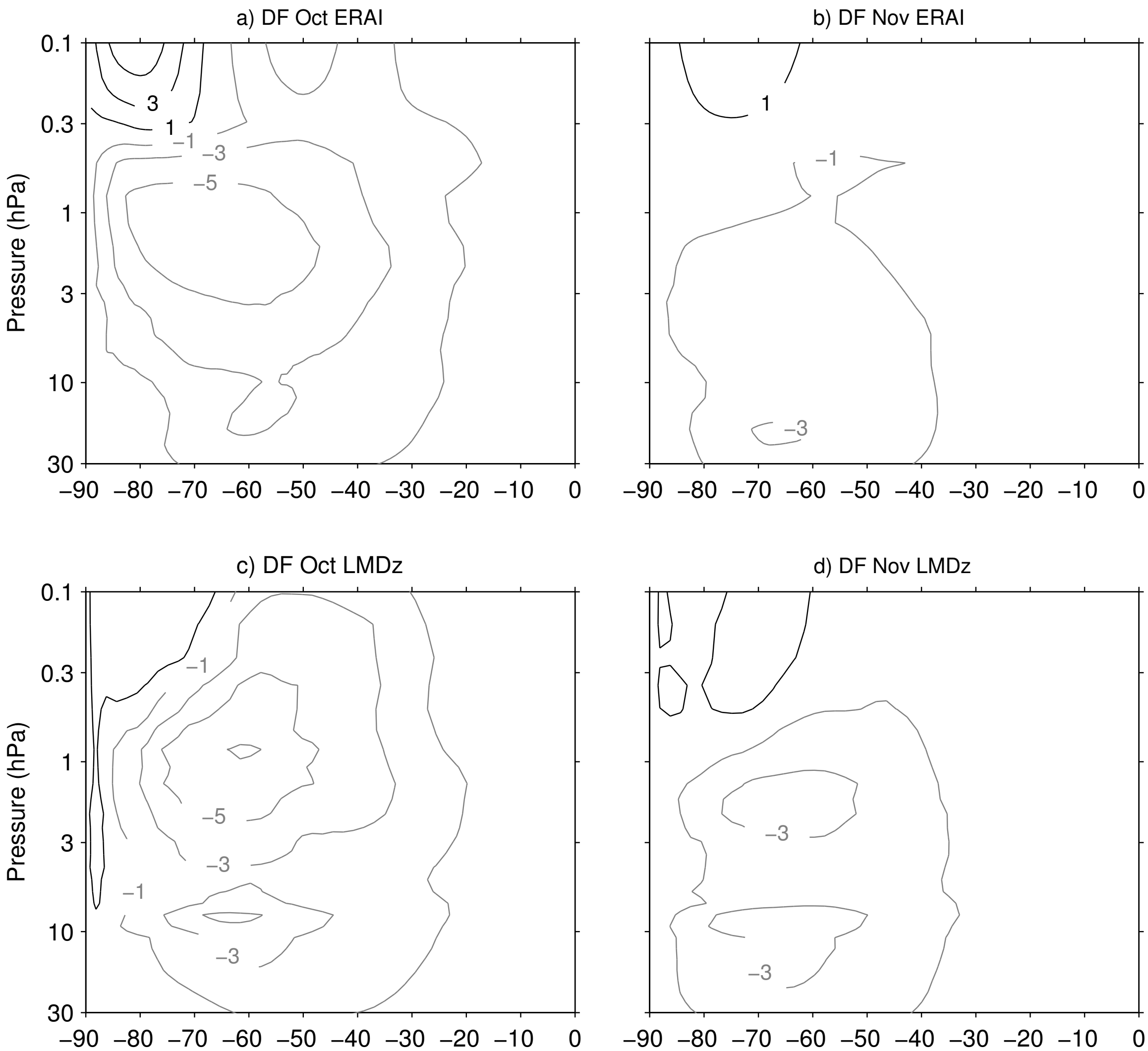


Figure 3: Latitude-height profiles of resolved wave drag for (a) October and (b) November for ERAI. (c, d) Same as (a, b) but for LMDz. Contour interval is 2 are $\mathrm{m{\cdot}s^{-1}{\cdot}day^{-1}}$, starting at $\pm 1$ $\mathrm{m{\cdot}s^{-1}{\cdot}day^{-1}}$.

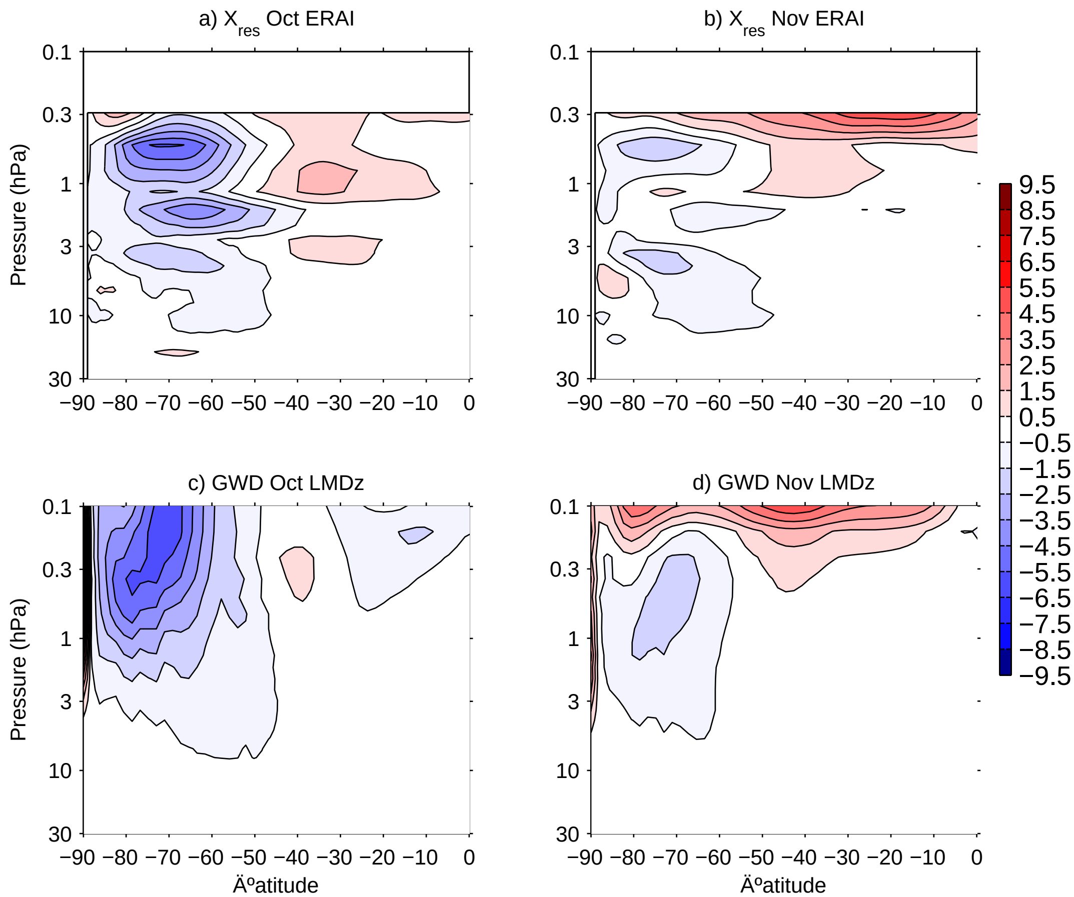


Figure 4: Same as Fig. 3, but for unresolved (parameterized) gravity waves.

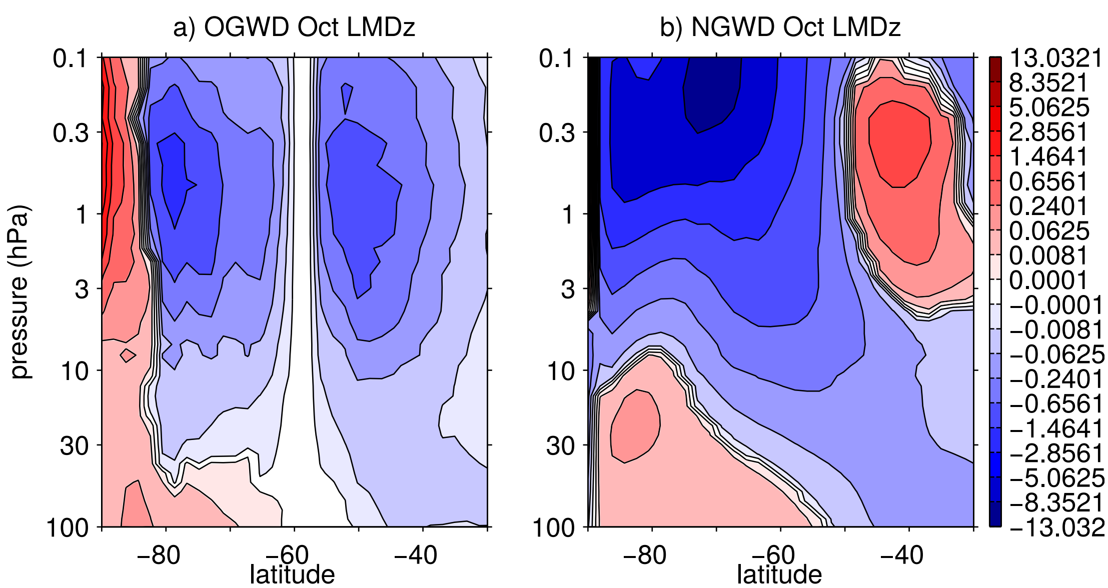


Figure 5: Latitude-height profiles in the stratosphere of (a) orographic, and (b) nonorographic gravity wave drag (in m·s$^{-1}$·day$^{-1}$) in LMDz for October.

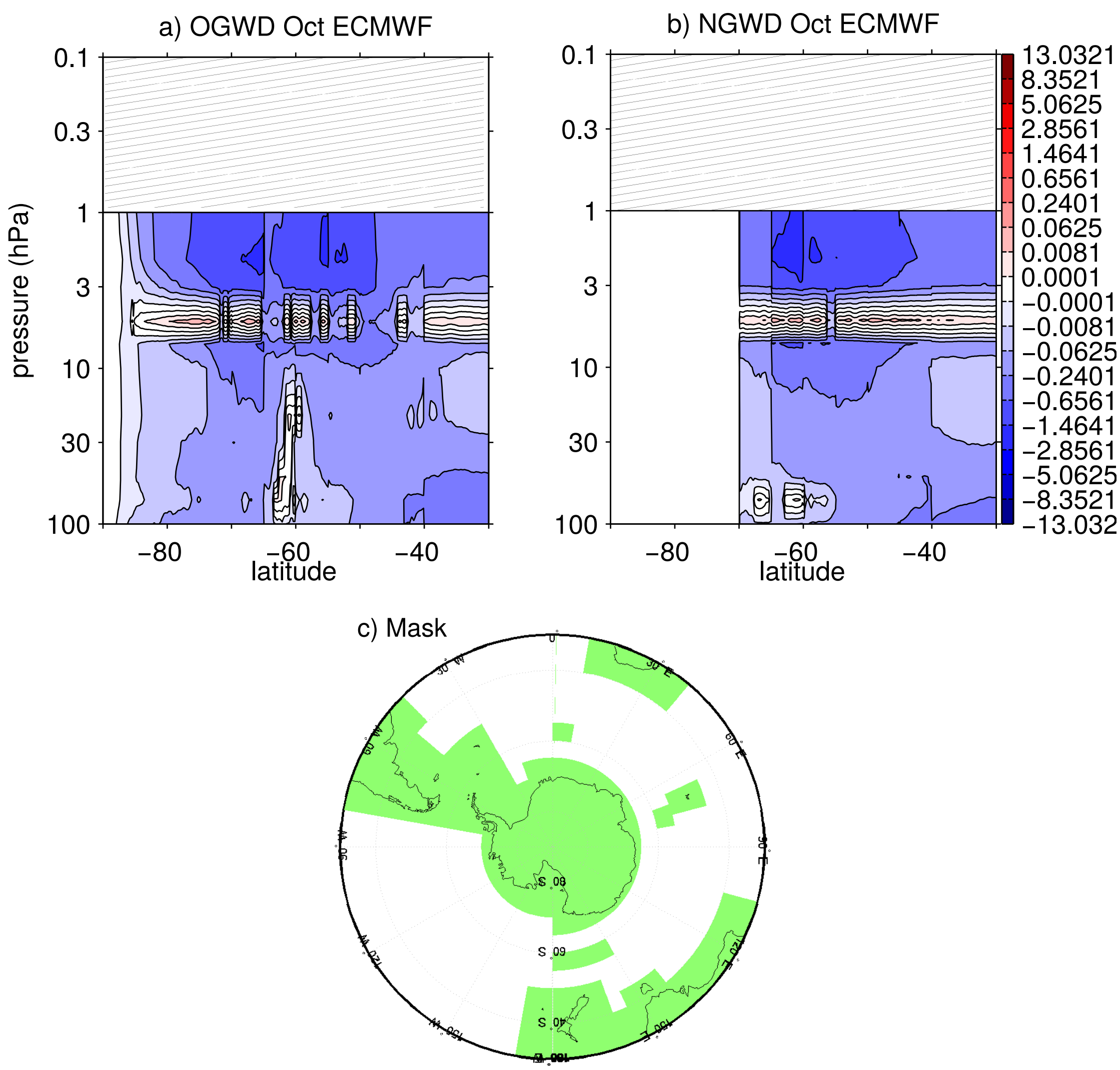


Figure 6: (a, b) As in Fig. 5, but for resolved gravity waves in the ECMWF operational analyses (2006–2010 period). Data is not displayed higher of 1 hPa (hatched area). (c) Map showing the continental mask (in green) used to discriminate orographic and nonorographic GWs in the ECMWF operational analyses data.

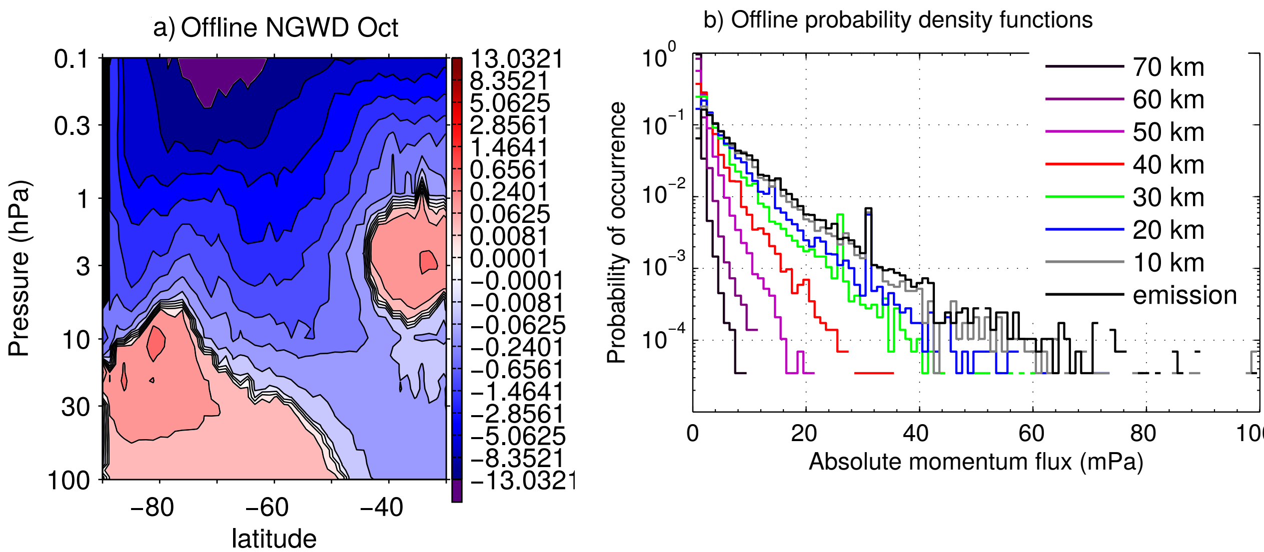


Figure 7: Some gravity wave diagnostics produced offline using LMDz fields for a given October: a) nonorographic gravity wave drag (in m·s$^{-1}$·day$^{-1}$), and b) probability density functions (histogram style) of NGW absolute momentum fluxes in the latitude band 90°S-40°S at different altitudes.

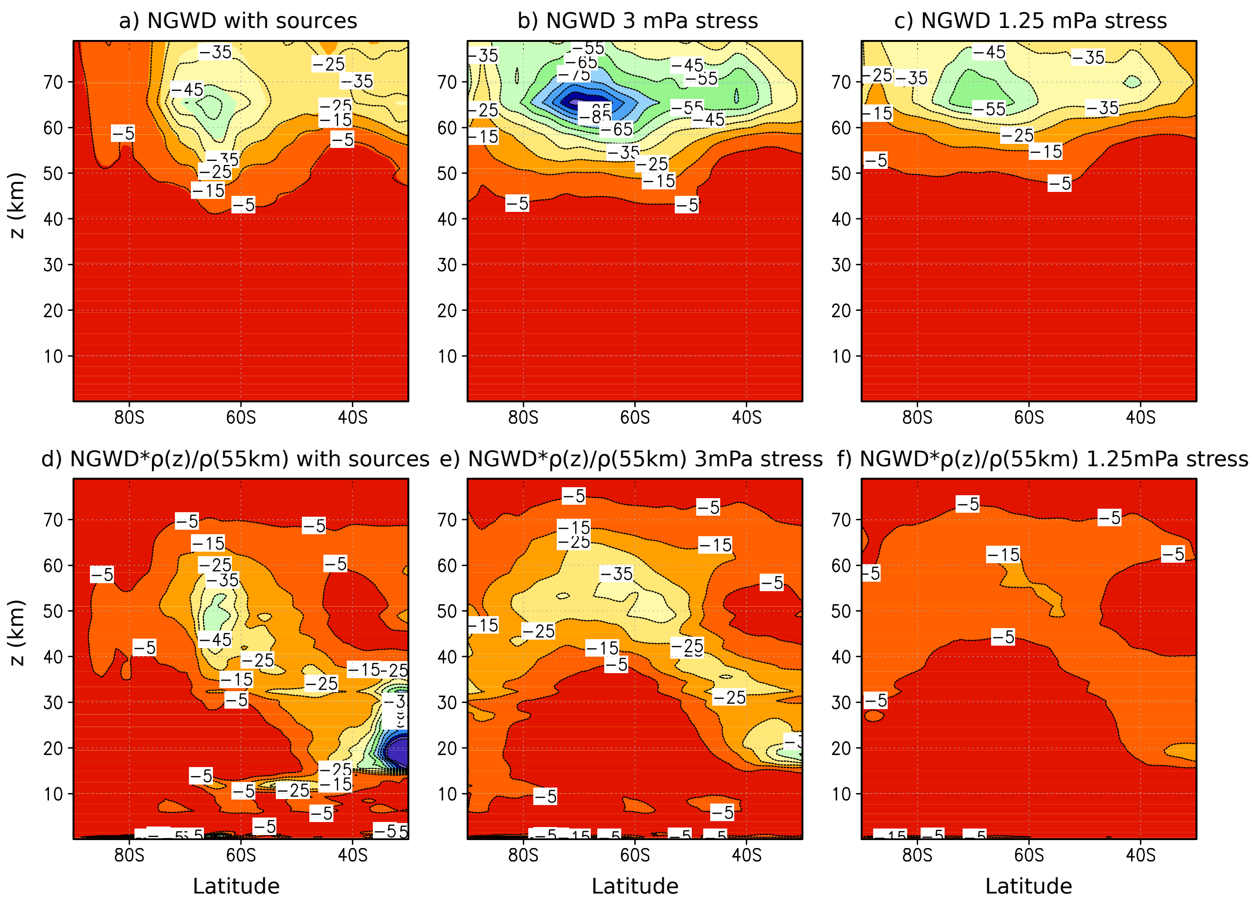


Figure 8: Westward nonorographic gravity wave drag (in m$\cdot$s$^{-1}\cdot$day$^{-1}$) derived offline using a) GW sources, b) a fixed emitted stress of 3 mPa, and c) a fixed emitted stress of 1.25 mPa. In order to emphasize the drag at stratospheric levels, the bottom panels display the drag scaled by a normalized density.